Available online at www.sciencedirect.com
ScienceDirect
Chaos, Solitons and Fractals 36 (2008) 828–842
CHAOS
SOLITONS & FRACTALS
www.elsevier.com/locate/chaos

Tensile-compressive asymmetry influence on shape memory alloy system dynamics

Marcelo A. Savi [a,*], Milton A.N. Sá [a], Alberto Paiva [b], Pedro M.C.L. Pacheco [c]

[a] *Universidade Federal do Rio de Janeiro, COPPE – Department of Mechanical Engineering, P.O. Box 68.503, 21.941.972 Rio de Janeiro, Brazil*
[b] *Universidade Federal Fluminense, Escola de Engenharia Industrial e Metalúrgica de Volta Redonda, 27.255.250 Volta Redonda, RJ, Brazil*
[c] *CEFET/RJ – Department of Mechanical Engineering, 20.271.110 Rio de Janeiro, RJ, Brazil*

Accepted 5 September 2006

Abstract

The remarkable properties of shape memory alloys (SMAs) are attracting much technological interest in several science and engineering fields, varying from medical to aerospace applications. Hysteretic response of these systems is one of their essential characteristics being related to the martensitic phase transformation. The dynamical response of systems with SMA actuators presents a rich behavior due to their intrinsic nonlinear characteristic. Since experimental results show that SMAs present an asymmetric behavior when subjected to tensile or compressive loads, it is important to evaluate the influence of this kind of behavior in the nonlinear dynamics of mechanical systems with SMA devices. This article discusses the nonlinear dynamics of shape memory alloy systems, considering the influence of tensile-compressive asymmetry in the thermomechanical behavior of SMAs. An iterative numerical procedure based on the operator split technique, the orthogonal projection algorithm and the fourth-order Runge–Kutta method is developed to deal with nonlinearities in the formulation. A numerical investigation is carried out showing some qualitative results such as chaotic-like response and multi-stability behavior for a single degree of freedom SMA oscillator.
© 2006 Elsevier Ltd. All rights reserved.

1. Introduction

The remarkable properties of shape memory alloys (SMAs) are attracting much technological interest in several science and engineering fields, varying from medical to aerospace applications. Machado and Savi [15,16] make a review on the most relevant SMA applications within orthodontics and biomedical areas. Engineering applications are also extensive [23]. They are ideally suited to be used as self-actuating fasteners, thermally actuator switches, seals, connectors and clamps [40]. Moreover, aerospace technology is also exploiting SMA properties in order to build self-erectable structures, stabilizing mechanisms, solar batteries, nonexplosive release devices and other possibilities [6,22]. Micromanipulators and robotics actuators have been conceived employing SMAs properties to mimic the smooth motions of

* Corresponding author.
E-mail addresses: savi@mecanica.ufrj.br (M.A. Savi), paiva@lavi.coppe.ufrj.br (A. Paiva), calas@cefet-rj.br (P.M.C.L. Pacheco).

0960-0779/$ - see front matter © 2006 Elsevier Ltd. All rights reserved.
doi:10.1016/j.chaos.2006.09.043

human muscles [9,43,27,11]. Furthermore, SMAs are being used as actuators for vibration and buckling control of flexible structures [3,27].

SMAs are materials that present, among other characteristics, the capacity of undergoing large residual deformations, and then, after a temperature increase, recover its original shape. SMAs are easy to manufacture, relatively lightweight, and able of producing high forces or displacements with low power consumption. The mechanism behind SMAs remarkable behavior is related to martensitic phase transformation that the alloy undergoes when subjected to stress and/or temperature changes, which may be accomplished by electrically heating the SMA. The two basic crystalline states that can occur are austenite and martensite. In martensitic phase, there are plates which may be internally twin-related, and different deformation orientations of crystallographic plates constitute what is known by martensitic variants. Hence, martensite can be either twinned or detwinned. The shape memory effect (SME) occurs at temperatures that are below a critical value, where twinned martensite is stable when free from stress. The conversion from twinned to detwinned martensite takes place by means of a loading process. When the loading–unloading process is finished, some amount of residual strain remains, meaning that the reverse transformation, from detwinned to twinned martensite, is not completed. The SME takes place by heating the alloy, which controls the transformation from detwinned martensite to austenite. At temperatures that are above another critical value, when a specimen of SMA is stressed at a constant temperature, inelastic deformation is observed above a critical stress. This inelastic process, however, may fully recover during the subsequent unloading. The stress–stain curve, which is the macroscopic manifestation of the deformation mechanism of the martensite, forms a hysteresis loop. This phenomenon is the pseudoelastic effect, which is also associated with phase transformations.

Hysteretic response of shape memory alloys is one of their essential characteristics. Basically, hysteresis loop may be observed either in stress–strain or in strain–temperature curves. The major (or external) hysteresis loop can be defined as the envelope of all minor (or internal) hysteresis loops, usually denoted as subloops. Macroscopic description of the SMA hysteresis loops, together with their subloops due to incomplete phase transformations, is an important aspect in the phenomenological description of the thermomechanical behavior of SMAs, being of great interest in technological applications [31].

The dynamical response of systems with SMA actuators presents a rich behavior due to their intrinsic nonlinear characteristic, being previously addressed in different references [39,38,8,5,30,28,29,37,42,7,19,14,10,35]. Various applications are exploiting SMAs' dynamical response. SMAs' nonlinear response is associated with both adaptive dissipation related to their hysteretic behavior and huge changes in their properties caused by phase transformations. Concerning the dissipation effect, SMAs' high damping capacity may be exploited in adaptive passive control employed in bridges and civil structures subjected to earthquakes, for example [10,4,41,42,30,29,20]. SMAs' property changes due to phase transformations, on the other hand, may exploit either forces or displacements generated by this phenomenon as well as natural frequencies and stiffness variations [42,25]. Chaotic behavior is also a possibility of SMA dynamical response discussed in different references [32,33,18,34,17,12,13,2]. Recently, some experimental analyses confirm the presence of chaos in shape memory systems [19].

Regarding the dynamical behavior of SMA oscillators, Savi and Braga [32] discuss the chaotic behavior of shape memory helical springs. Machado et al. [18] discuss bifurcation and crises in a shape memory oscillator. Savi and Pacheco [34] study some characteristics of shape memory oscillators with one and two-degree of freedom, showing the existence of chaos and hyperchaos in these systems. Machado et al. [17] revisited the analysis of coupled shape memory oscillators, considering two-degree of freedom oscillators. All these articles employ a polynomial constitutive model to describe the thermomechanical behavior of SMAs. Savi and Braga [33] also study shape memory oscillators employing another constitutive model to describe the restitution force provided by a shape memory helical spring.

This article deals with the nonlinear dynamics of shape memory systems where the restitution force is described by a constitutive model with internal constraints [24]. This constitutive model presents close agreement with experimental data and therefore, can represent more accurately the qualitative behavior previously analyzed in the cited references, which use a simpler constitutive model. The accurate representation of the SMA hysteresis is critical to the nonlinear dynamics analysis and allows more realistic description of important characteristics as the adaptive dissipation influence in the system dynamics [2]. Since experimental results show that SMAs present an asymmetric behavior when subjected to tensile or compressive loads, it is important to evaluate the influence of this kind of behavior in the nonlinear dynamics of mechanical systems with SMA devices. The constitutive model employed in this article allows one to capture this important issue.

An iterative numerical procedure based on the operator split technique [21], the orthogonal projection algorithm [36] and the fourth-order Runge–Kutta method is developed to deal with nonlinearities in the formulation. Numerical investigation is carried out showing some characteristics of SMA dynamical response. Tensile-compressive asymmetry is of concern, discussing some differences introduced by this consideration.

2. Constitutive model

There are different ways to describe the thermomechanical behavior of SMAs. Here, a constitutive model that is built upon the Fremond's model and previously presented in different references [36,1,24] is employed. This model considers different material properties and four macroscopic phases for the description of the SMA behavior. The tension-compression asymmetry is taken into account. Moreover, the model also considers plastic strain and plastic-phase transformation coupling, which allows the two-way shape memory effect description. Nevertheless, for the sake of simplicity, these two characteristics are not considered in this article.

Therefore, besides strain (ε) and temperature (T), the model considers four more state variables associated with the volumetric fraction of each phase: β_1 is associated with tensile detwinned martensite, β_2 is related to compressive detwinned martensite, β_3 represents austenite and β_4 corresponds to twinned martensite. A free energy potential is proposed concerning each isolated phase. After this definition, a free energy of the mixture can be written weighting each energy function with its volumetric fraction. With this assumption, it is possible to obtain a complete set of constitutive equations that describes the thermomechanical behavior of SMAs as presented below:

$$\sigma = E\varepsilon + (\alpha^{C} + E\alpha_{h}^{C})\beta_2 - (\alpha^{T} + E\alpha_{h1}^{T})\beta_1 - \Omega(T - T_0), \tag{1}$$

$$\dot{\beta}_1 = \frac{1}{\eta_1}\left\{\alpha^{T}\varepsilon + \Lambda_1 + \beta_2\left(\alpha_{h}^{C}\alpha^{T} + \alpha_{h}^{T}\alpha^{C} + E\alpha_{h}^{T}\alpha_{h}^{C}\right) - \beta_1\left(2\alpha_{h}^{T}\alpha^{T} + E\alpha_{h}^{T^2}\right) + \alpha_{h}^{T}[E\varepsilon - \Omega(T - T_0)] - \partial_1 J_\pi\right\} + \partial_1 J_\chi, \tag{2}$$

$$\dot{\beta}_2 = \frac{1}{\eta_2}\left\{-\alpha^{C}\varepsilon + \Lambda_2 + \beta_1\left(\alpha_{h}^{T}\alpha^{C} + \alpha_{h}^{C}\alpha^{T} + E\alpha_{h}^{C}\alpha_{h}^{T}\right) - \beta_2\left(2\alpha_{h}^{C}\alpha^{C} + E\alpha_{h}^{C^2}\right) - \alpha_{h}^{C}[E\varepsilon - \Omega(T - T_0)] - \partial_2 J_\pi\right\} + \partial_2 J_\chi, \tag{3}$$

$$\dot{\beta}_3 = \frac{1}{\eta_3}\left\{-\frac{1}{2}(E_A - E_M)\left(\varepsilon + \alpha_{h}^{C}\beta_2 - \alpha_{h}^{T}\beta_1\right)^2 + \Lambda_3 + (\Omega_A - \Omega_M)(T - T_0)\left(\varepsilon + \alpha_{h}^{C}\beta_2 - \alpha_{h}^{T}\beta_1\right) - \partial_3 J_\pi\right\} + \partial_3 J_\chi, \tag{4}$$

where $E = E_M + \beta_3(E_A - E_M)$ is the elastic modulus while $\Omega = \Omega_M + \beta_3(\Omega_A - \Omega_M)$ is related to the thermal expansion coefficient. Notice that subscript "A" refers to austenitic phase, while "M" refers to martensite. Besides, different properties are assumed to consider tension-compression asymmetry, where the superscript "T" refers to tensile while "C" is related to compressive properties. Moreover, parameters $\Lambda_1 = \Lambda_1(T)$, $\Lambda_2 = \Lambda_2(T)$ and $\Lambda_3 = \Lambda_3(T)$ are associated with phase transformations stress levels. Parameter α_h is introduced in order to define the horizontal width of the stress–strain hysteresis loop, while α helps vertical hysteresis loop control on stress–strain diagrams.

The terms $\partial_n J_\pi$ ($n = 1,2,3$) are sub-differentials of the indicator function J_π with respect to β_n [26]. The indicator function $J_\pi(\beta_1,\beta_2,\beta_3)$ is related to a convex set π, which provides the internal constraints related to the phases' coexistence. With respect to evolution equations of volumetric fractions, η_1, η_2 and η_3 represent the internal dissipation related to phase transformations. Moreover $\partial_n J_\chi$ ($n = 1,2,3$) are sub-differentials of the indicator function J_χ with respect to $\dot{\beta}_n$ [26]. This indicator function is associated with the convex set χ, which establishes conditions for the correct description of internal subloops due to incomplete phase transformations and also avoids phase transformations M+ → M or M− → M.

Concerning the parameters definition, linear temperature dependent relations are adopted for Λ_1, Λ_2 and Λ_3 as follows:

$$\Lambda_1 = -L_0^{T} + \frac{L^{T}}{T_M}(T - T_M), \quad \Lambda_2 = -L_0^{C} + \frac{L^{C}}{T_M}(T - T_M), \quad \Lambda_3 = -L_0^{A} + \frac{L^{A}}{T_M}(T - T_M). \tag{5}$$

Here, T_M is the temperature below which the martensitic phase becomes stable. Besides, L_0^{T}, L^{T}, L_0^{C}, L^{C}, L_0^{A} and L^{A} are parameters related to critical stress for phase transformation, remembering that the indexes "T" refers to tensile, "C" to compression and "A" to austenite.

In order to contemplate different characteristics of the kinetics of phase transformation for loading and unloading processes, it is possible to consider different values to the parameter η_n ($n = 1,2,3$), which is related to internal dissipation: η_n^{L} and η_n^{U} during loading and unloading process, respectively. For more details about the constitutive model, see [24,31].

3. Shape memory oscillator

The dynamical behavior of SMAs is analyzed by considering a single-degree of freedom oscillator, which consists of a mass m attached to a shape memory element of length L and cross-section area A. A linear viscous damper, associated with a parameter c, is also considered (Fig. 1). The system is harmonically excited by a force $F = F_0\sin(\omega t)$.

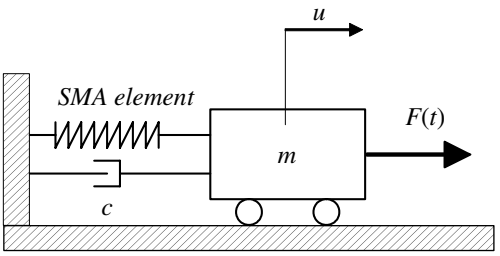

Fig. 1. Shape memory oscillator.

With these assumptions, equation of motion may be formulated by considering the balance of linear momentum, assuming that the restitution force is provided by a SMA element described by the constitutive equation presented in the previous section. Therefore, the following equation of motion is obtained:

$$m\ddot{u} + c\dot{u} + K = F_0 \sin(\omega t). \tag{6}$$

Notice that the restitution force may be expressed as $K = \sigma A$. Using the constitutive equation for SMAs, one writes

$$m\ddot{u} + c\dot{u} + EA\varepsilon + (A\alpha^{C} + EA\alpha_h^{C})\beta_2 - (A\alpha^{T} + EA\alpha_h^{T})\beta_1 - \Omega A(T - T_0) = F_0 \sin(\omega t). \tag{7}$$

In order to obtain a dimensionless equation of motion, system's parameters are defined as follows:

$$\omega_0^2 = \frac{E_R A}{mL}; \quad \xi = \frac{c}{m\omega_0}; \quad \bar{\alpha}^{C,T} = \frac{\alpha^{C,T} A}{mL\omega_0^2} = \frac{\alpha^{C,T}}{E_R}; \quad \bar{\alpha}_h^{C,T} = \frac{\alpha_h^{C,T} E_R A}{mL\omega_0^2} = \alpha_h^{C,T}; \quad \delta = \frac{F_0}{mL\omega_0^2} = \frac{F_0}{E_R A};$$
$$\bar{\Omega} = \frac{\Omega_R A T_R}{mL\omega_0^2} = \frac{\Omega_R T_R}{E_R}; \quad \mu_E = \frac{E}{E_R}; \quad \mu_\Omega = \frac{\Omega}{\Omega_R}; \quad \varpi = \frac{\omega}{\omega_0}. \tag{8}$$

These definitions allow one to define the following dimensionless variables, respectively related to mass displacement (U), temperature (θ) and time (τ):

$$U = \frac{u}{L}; \quad \theta = \frac{T}{T_R}; \quad \tau = \omega_0 t. \tag{9}$$

Notice that dimensionless parameters and variables are defined considering some reference values for temperature dependent parameters. This is done assuming a reference temperature, T_R, where these parameters are evaluated. Therefore, parameters with subscript R are evaluated in this reference temperature. The dimensionless equation of motion has the form

$$U'' + \xi U' + \mu_E U + (\bar{\alpha}^{C} + \mu_E \bar{\alpha}_h^{C})\beta_2 - (\bar{\alpha}^{T} + \mu_E \bar{\alpha}_h^{T})\beta_1 - \mu_\Omega \bar{\Omega}(\theta - \theta_0) = \delta \sin(\varpi\tau), \tag{10}$$

where derivatives with respect to dimensionless time are represented by $(\,)' = \mathrm{d}(\,)/\mathrm{d}\tau$. This equation of motion can be written in terms of a system of first-order differential equations as follows:

$$\begin{aligned} x' &= y, \\ y' &= \delta \sin(\varpi\tau) - \xi y - \mu_E x - \left(\bar{\alpha}^{C} + \mu_E \bar{\alpha}_h^{C}\right)\beta_2 + \left(\bar{\alpha}^{T} + \mu_E \bar{\alpha}_h^{T}\right)\beta_1 + \mu_\Omega \bar{\Omega}(\theta - \theta_0). \end{aligned} \tag{11}$$

In order to deal with nonlinearities of these equations of motion, an iterative procedure based on the operator split technique [21] is employed. With this assumption, the fourth-order Runge–Kutta method is used together with the projection algorithm proposed in [36] to solve the constitutive equations. The solution of the constitutive equations also employs the operator split technique together an *implicit Euler* method. For β_n ($n = 1, 2, 3$) calculation, the evolution equations are solved in a decoupled way. At first, the equations (except for the sub-differentials) are solved using an iterative *implicit Euler* method. If the estimated results obtained for β_n does not satisfy the imposed constraints, an *orthogonal projection algorithm* pulls their value to the nearest point on the domain's surface [24].

4. Numerical simulations

This section presents some numerical simulations developed in order to show the qualitative behavior of SMA dynamical responses. In all simulations, it is considered parameters presented in Table 1 and it is also assumed a unitary mass and a SMA element with $A = 1.96 \times 10^{-5}$ m and $L = 50 \times 10^{-3}$ m. Fig. 2(a) presents a quasi-static stress–strain

Table 1
SMA parameters

E_A (GPa)	E_M (GPa)	α^T (MPa)	α^C (MPa)	ε_R^T	ε_R^C	L_0^T (MPa)	L^T (MPa)	L_0^C (MPa)	L^C (MPa)	L_0^A (MPa)
54	42	150	165	0.0555	−0.035	0.15	41.5	0.17	96.2	0.63
L^A (MPa)	Ω_A (MPa/K)	Ω_M (MPa/K)	T_M (K)	T_A (K)	η_1^L (MPa s)	η_1^U (MPa s)	η_2^L (MPa s)	η_2^U (MPa s)	η_3^L (MPa s)	η_3^U (MPa s)
185	0.74	0.17	291.4	307.5	10	27	10	27	10	27

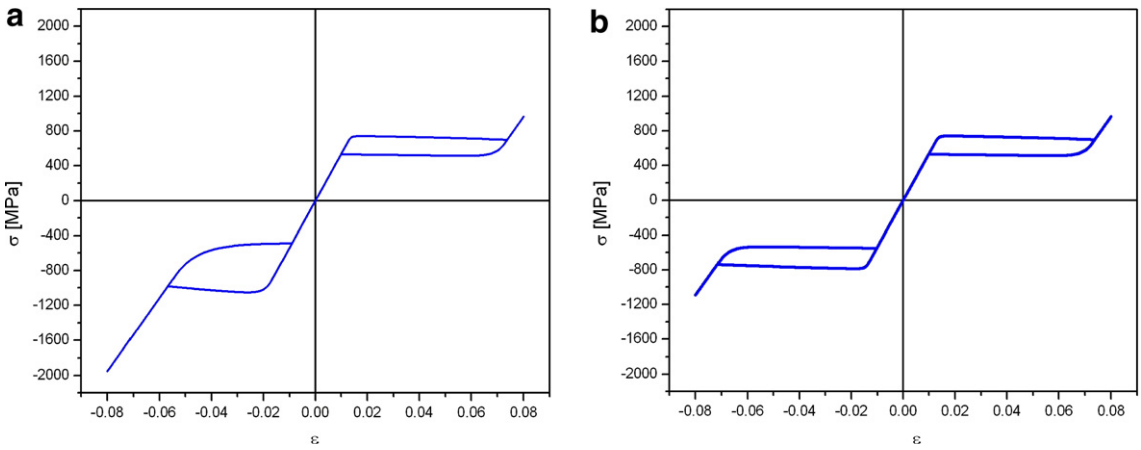

Fig. 2. Stress–strain curve for a high temperature ($T = 373$ K). (a) Asymmetric case; (b) symmetric case.

curve obtained with the adjusted parameters for a high temperature ($T = 373$ K, where austenite is stable for a stress-free state). It is noticeable the tensile-compressive asymmetry, which represents a characteristic of SMA thermomechanical behavior. In order to analyze the effect of this asymmetric characteristic, it is also considered a situation with tensile-compressive symmetry, assuming tensile properties values to both tensile and compressive stress states (Fig. 2(b)).

4.1. Free vibration

At first, free vibration is focused on, by letting δ vanish in the dimensionless equations of motion. It is assumed that reference parameters (E_R, Ω_R) are evaluated in the reference temperature $T_R = T_M$, that is, $E_R = E_M$, $\Omega_R = \Omega_M$. The system has different equilibrium points depending on temperature. The oscillator free response is illustrated analyzing a system without viscous damping ($\xi = 0$). Results from simulations are presented in the form of phase portraits. In order to establish a comparison between the dynamical response of symmetric and asymmetric systems, tensile-compressive symmetry are considered assuming tensile parameters listed in Table 1 to both tensile and compression behaviors. Fig. 3 presents the free response of a system with tensile-compressive symmetry, at different temperatures: $\theta = 1.28$, representing a high temperature where austenite is stable for a stress-free state; and $\theta = 0.99$, a low temperature where martensite is stable for a stress-free state. Between these two temperatures, martensite and austenite may coexist and it represents a transition region between the two cited situations [34,17,18]. For high temperatures, there is only a single equilibrium point. The system response presents dissipation for high amplitudes, converging to an elastic orbit near the equilibrium point, where phase transformations do not take place anymore. This behavior is due to hysteresis loop and the absence of energy dissipation in the linear-elastic region. For low temperatures, the dissipation characteristics are similar to the high temperature behavior but there is an increase in the number of equilibrium points. By observing the phase portrait, it is noticeable three stable equilibrium points, related to different martensitic variants (a stable point has a positive displacement, which is denoted as a positive equilibrium point, while a stable point that has a negative displacement is denoted as a negative equilibrium point; besides, there is a null equilibrium point at the origin), and it is possible to infer about the existence of unstable points among the stable ones.

By considering the tensile-compressive asymmetry, phase portraits are deformed (Fig. 4). For low temperature case, it is noticeable that the position of the negative equilibrium point is closer to the origin (when compared to the symmetric case), which causes differences in the dynamical response.

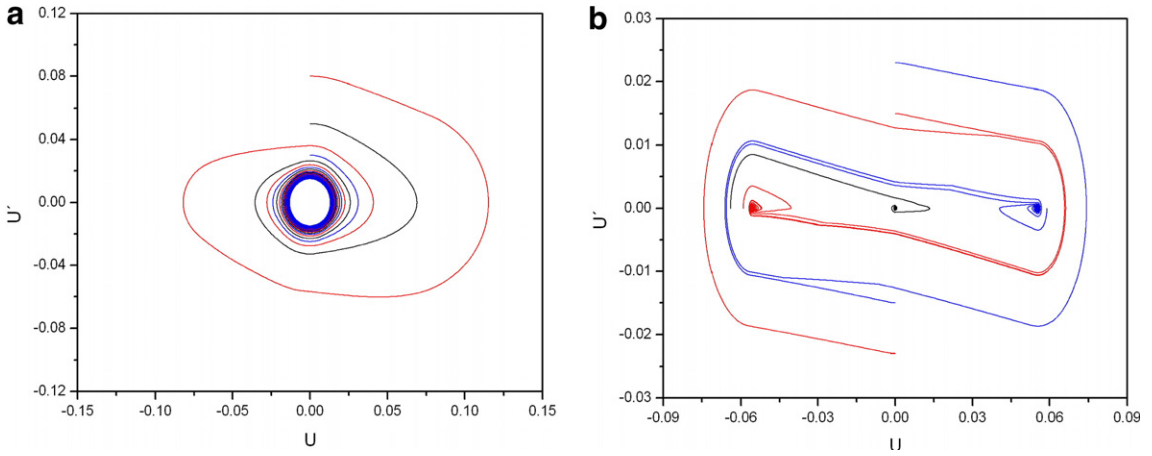

Fig. 3. Phase portrait for symmetric problem and different temperatures. (a) $\theta = 1.28$ and (b) $\theta = 0.99$.

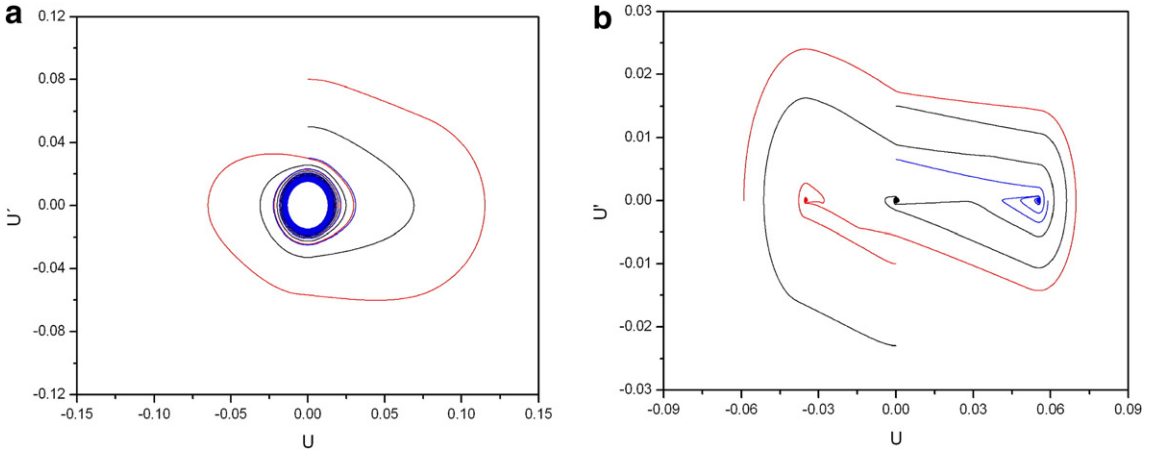

Fig. 4. Phase portrait for asymmetric problem and different temperatures. (a) $\theta = 1.28$ and (b) $\theta = 0.99$.

Figs. 5 and 6 present the free symmetric response for two situations related to high and low temperatures, respectively. The dynamical response shows a dissipative behavior stage of the system while it passes through the hysteresis loop region. After this stage, it stabilizes in an elastic orbit where there is no phase transformation. Since for low temperatures the system has different stable equilibrium points, it can stabilize in different positions, depending on initial conditions. Analogous responses can be achieved for asymmetric cases.

The existence of different equilibrium points may be exploited together with the temperature dependence in various applications. It is worthwhile to notice that temperature variations cause changes in the system position. In order to illustrate this behavior, it is shown a symmetric simulation where temperature varies as indicated in Fig. 7(a), by increasing system temperature between two levels. Fig. 7(b) and (c) shows the system response, presenting time history and phase space, respectively. Notice that the system oscillates around one point at low temperature, changing its oscillation position when temperature increases. This simulation illustrates the potentiality of SMA to be used as actuators for position control.

4.2. Forced vibration

The behavior of the forced system is far more complex. In order to start this analysis, it is discussed the high temperature behavior exploiting the idea of the intelligent dissipation due to hysteresis loop. A paradigmatic way to visualize this kind of behavior is obtained by considering the system response under resonant conditions. Hence, an

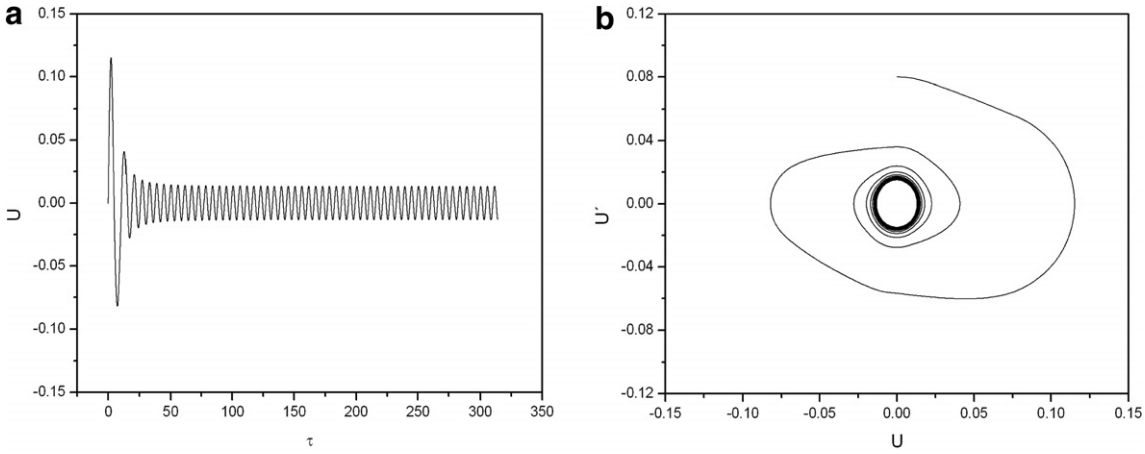

Fig. 5. Free vibration symmetric response for high temperature. (a) Time history and (b) phase space.

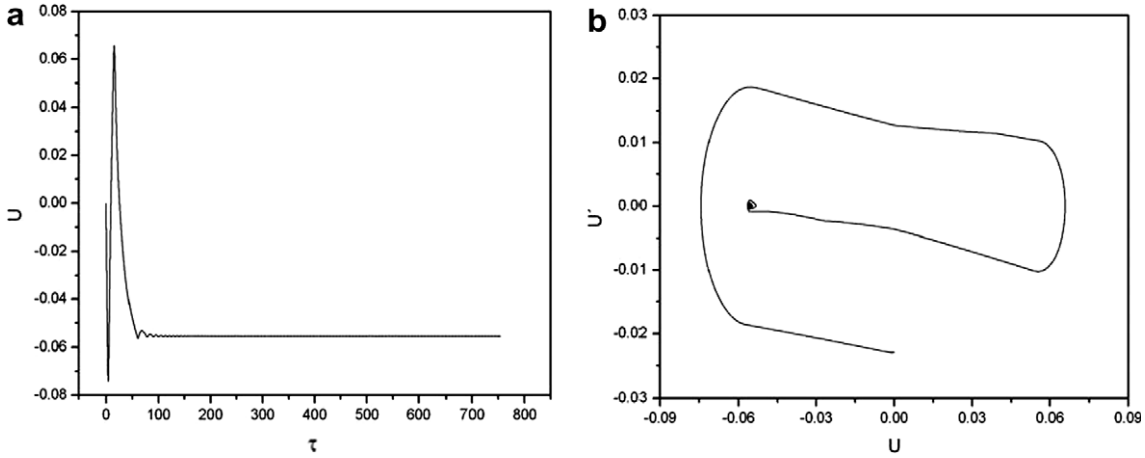

Fig. 6. Free vibration symmetric response for low temperature. (a) Time history and (b) phase space.

asymmetric condition is employed together with parameters $\xi = 0$, $\varpi = 1$, and $\theta = 1.28$. Moreover, austenitic properties are used as reference values ($T_R = T_A$, $E_R = E_A$, $\Omega_R = \Omega_A$). As it is well-known, a nondissipative linear system (where SMA element is replaced by a linear element) tends to increase the response amplitude indefinitely under this condition (Fig. 8(a)). The shape memory alloy system, on the other hand, tends to dissipate higher energy levels as the response amplitude grows. This is due to phase transformation related to hysteresis loop and therefore, the amplitude tends to stabilize in lower values, as shown in Fig. 8(b). This behavior is interesting to be exploited as a passive vibration control.

At this point, low temperature behavior (where martensite is stable for a stress-free state) is of concern. Therefore, it is assumed that reference parameters (E_R, Ω_R) are evaluated in the reference temperature $T_R = T_M$, that is, $E_R = E_M$, $\Omega_R = \Omega_M$. Moreover, it is assumed that $\xi = 5 \times 10^{-6}$, $\varpi = 1$, and $\theta = 0.99$. At first, a system with symmetric tensile-compressive behavior is focused on. In order to perform a global analysis, bifurcation diagrams are constructed, sampling the position against the slow quasi-static variation of the forcing amplitude parameter. Fig. 9 shows bifurcation diagrams obtained using two different procedures. The first considers similar initial conditions for each parameter value (Fig. 9(a)) while the second procedure considers stabilized values of state variables as initial conditions for the next parameter value (Fig. 9(b)). The second procedure is not capable to capture the coexistence of different attractors which is noticeable in a chaotic region of Fig. 9(a) that does not appear in Fig. 9(b), defined by a cloud of points between $\delta = 2 \times 10^{-3}$ and $\delta = 5 \times 10^{-3}$.

By observing the bifurcation diagram it is noticeable that there are periodic responses for low values of forcing parameters. By changing the forcing characteristics, it is possible to observe different kinds of response. Fig. 10 shows

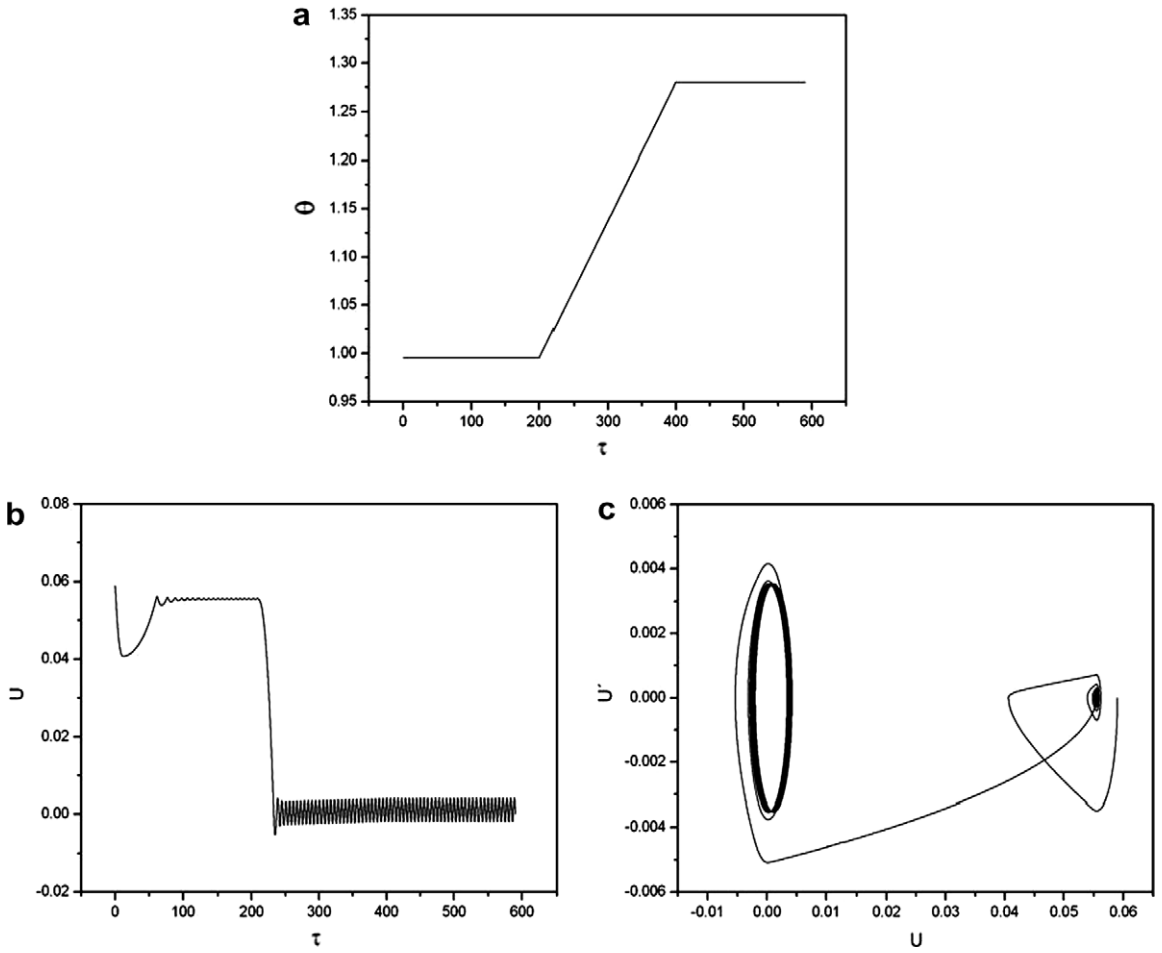

Fig. 7. Free vibration symmetric response due to temperature variations. (a) Temperature history, (b) time history and (c) phase space.

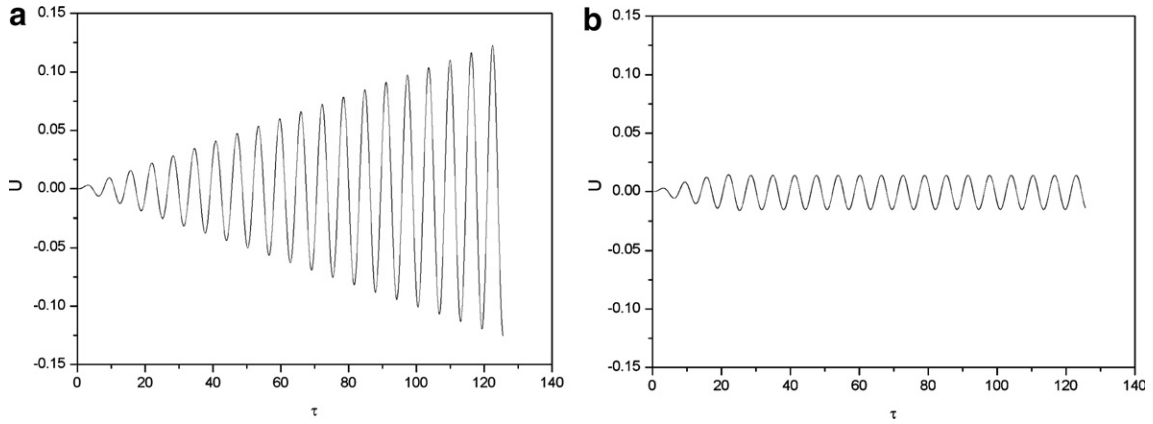

Fig. 8. Passive control exploiting hysteresis dissipation. (a) Linear element; (b) SMA element.

a chaotic-like response when $\delta = 3 \times 10^{-3}$ and for a larger forcing amplitude, $\delta = 8 \times 10^{-3}$, a chaotic-response with different pattern occurs, as shown in Fig. 11.

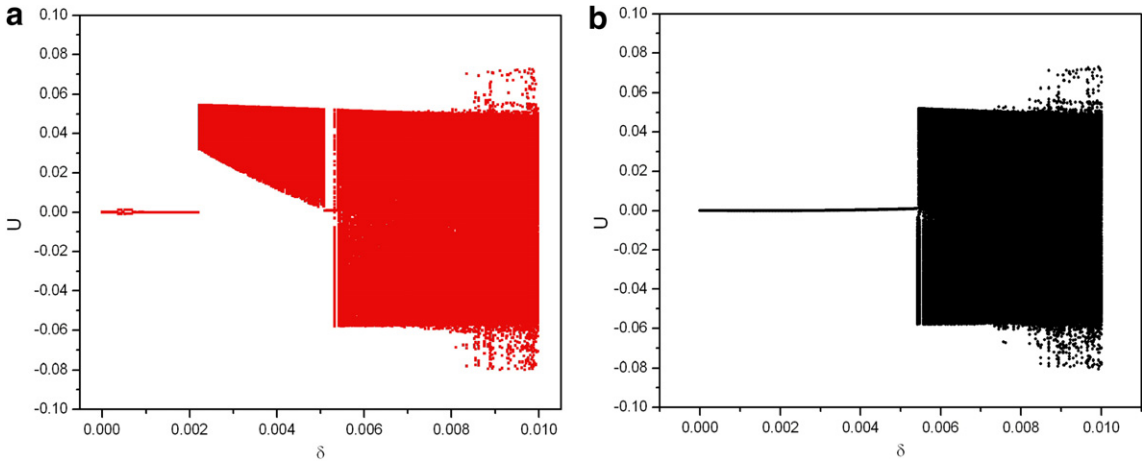

Fig. 9. Symmetric bifurcation diagrams for $\xi = 5 \times 10^{-6}$ and $\varpi = 1$. (a) Similar initial conditions for each parameter and (b) stabilized values of state variables as an initial condition for the next parameter value.

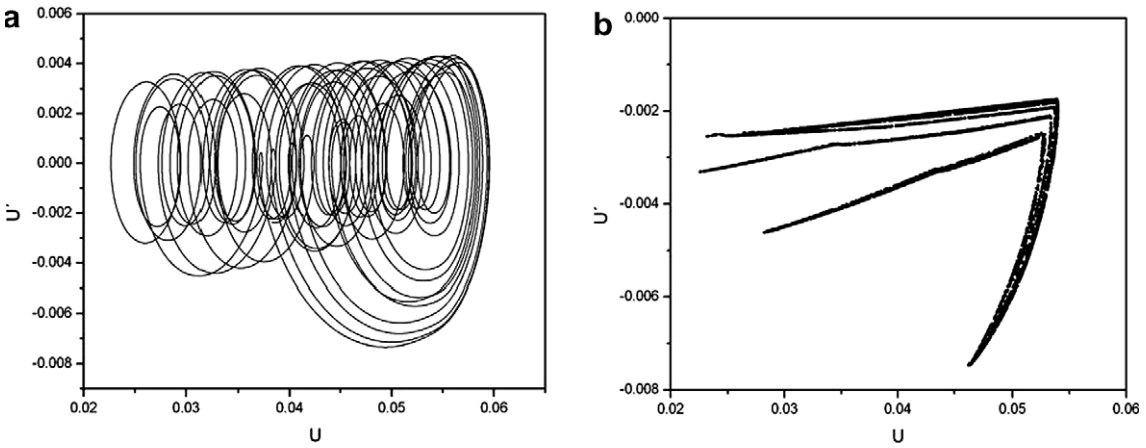

Fig. 10. Symmetric chaotic-like response for $\delta = 3 \times 10^{-3}$. (a) Phase state and (b) Poincaré map.

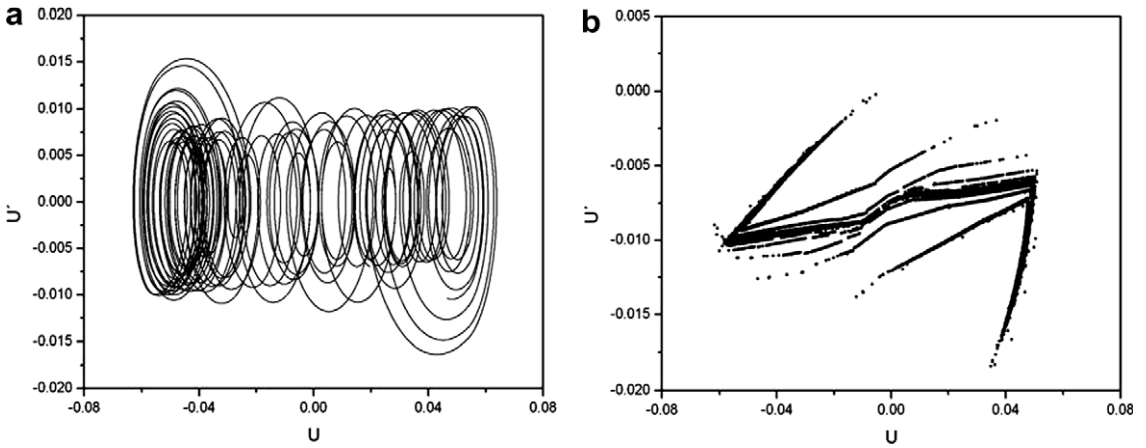

Fig. 11. Symmetric chaotic-like response for $\delta = 8 \times 10^{-3}$. (a) Phase state and (b) Poincaré map.

The fractal structure of chaotic-like attractors may be altered by changing dissipation characteristics. Fig. 12 shows this change for different values of parameter ξ considering a forcing amplitude of $\delta = 3 \times 10^{-3}$. Basically, three values are considered, showing that the dissipation increase tends to decrease the attractor dimension: 5×10^{-6}, 5×10^{-2}, 1×10^{-1}. Nevertheless, it should be pointed out that dissipation due to hysteresis loop is preponderant.

Transient responses and multi-stability are other interesting characteristics related to shape memory oscillators. Bifurcation diagrams presented in Fig. 9 shows cloud of points that appears just when the bifurcation diagram is constructed considering the same initial conditions for each value of control parameter δ (Fig. 9(a)). The other diagram (Fig. 9(b)) does not present this cloud of points since it is not capable to capture multi-stability characteristics. It is important to observe that, actually, there are three coexisting steady state solutions related to this region (a symmetric cloud of points can be obtained changing initial conditions of the bifurcation diagram of Fig. 9(a)). The forthcoming analysis exploits this coexisting attractors multi-stability by changing initial conditions and assuming $\delta = 3 \times 10^{-3}$, $\varpi = 1$ and $\xi = 5 \times 10^{-6}$. A period-1 response may be obtained considering initial conditions near the steady state solution presented in Fig. 9(b). Under this condition, the system oscillates around the null equilibrium point (Fig. 13). By assuming initial conditions within the cloud of points presented in Fig. 9(a), a chaotic-like response occurs. This type of response is related to oscillations in the positive part of phase space, and therefore, it is called positive chaotic-like response (Fig. 14). Finally, the third steady state response may be obtained assuming initial conditions within the symmetric cloud of point (not shown in Fig. 9(a)). Under this condition, the system presents a negative chaotic-like response that occurs in the negative part of phase space (Fig. 15).

The tensile-compressive asymmetry is now considered. Fig. 16 shows bifurcation diagrams obtained considering similar initial conditions for each parameter value (similar procedure employed to obtain Fig. 9(a)). Two different initial

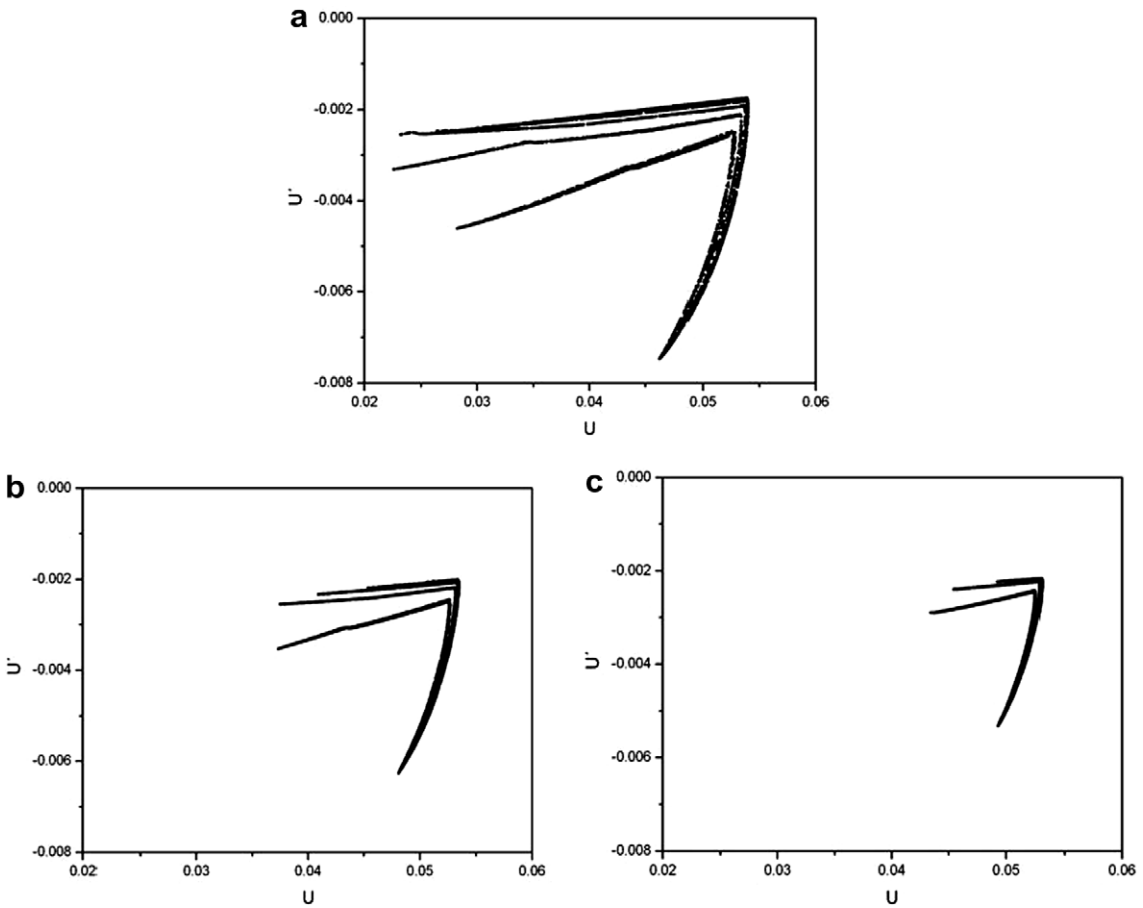

Fig. 12. Chaotic-like symmetric attractors by different dissipation parameters: (a) $\xi = 5 \times 10^{-6}$, (b) $\xi = 5 \times 10^{-2}$, (c) $\xi = 1 \times 10^{-1}$.

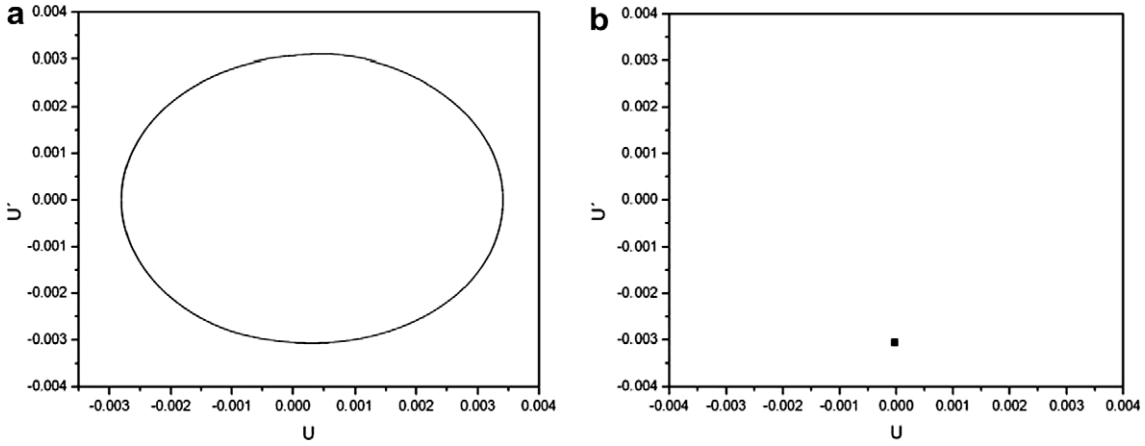

Fig. 13. Multi-stability: period-1symmetric response.

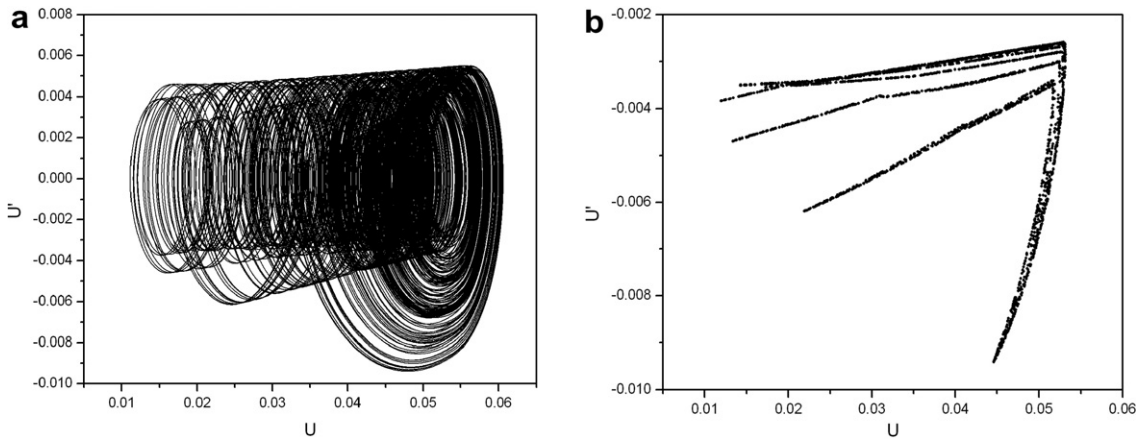

Fig. 14. Multi-stability: positive symmetric chaotic-like response.

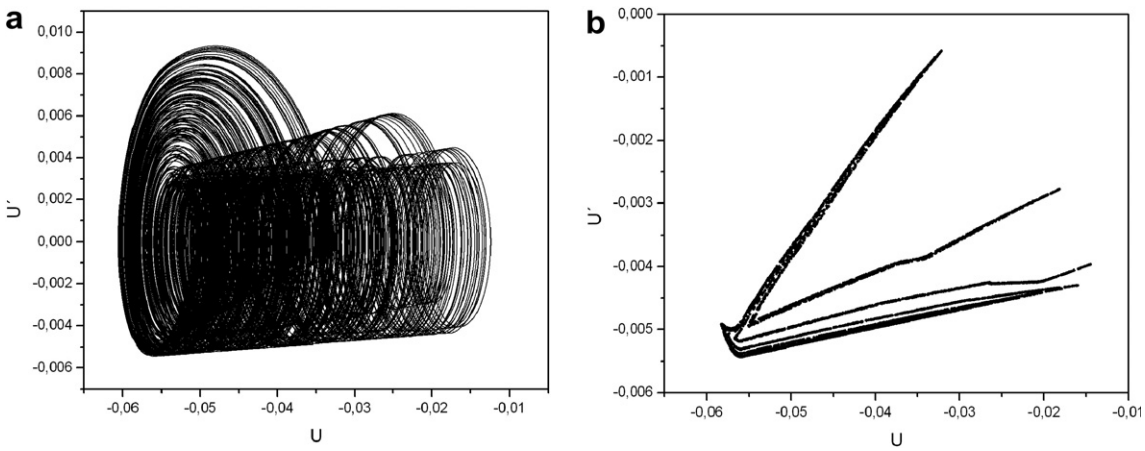

Fig. 15. Multi-stability: negative symmetric chaotic-like response.

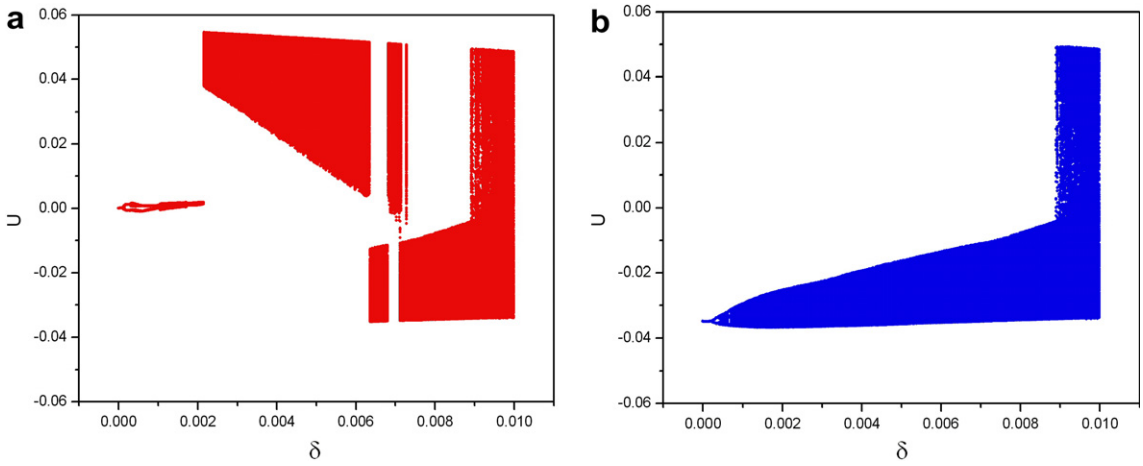

Fig. 16. Asymmetric bifurcation diagrams for $\xi = 5 \times 10^{-6}$, $\varpi = 1$ and $\theta = 0.99$ and different initial conditions.

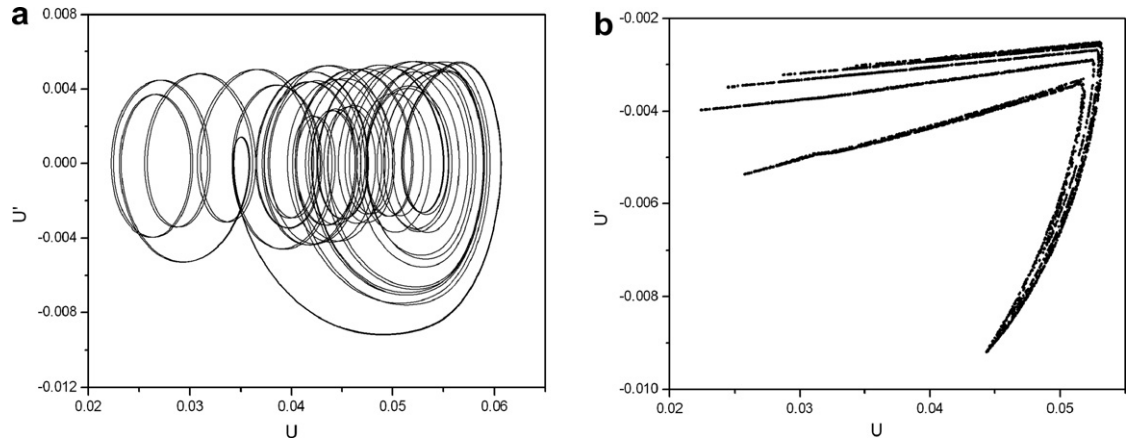

Fig. 17. Multi-stability: positive asymmetric chaotic-like response.

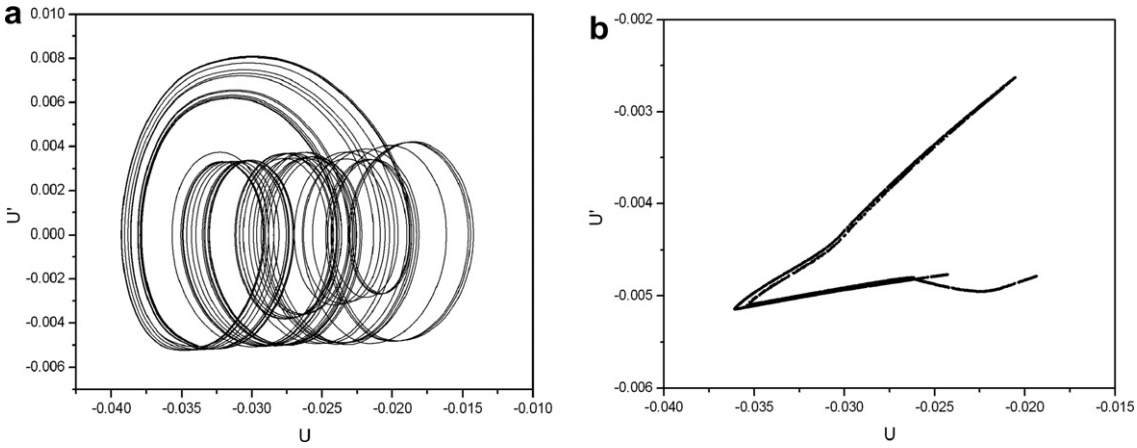

Fig. 18. Multi-stability: negative asymmetric chaotic-like response.

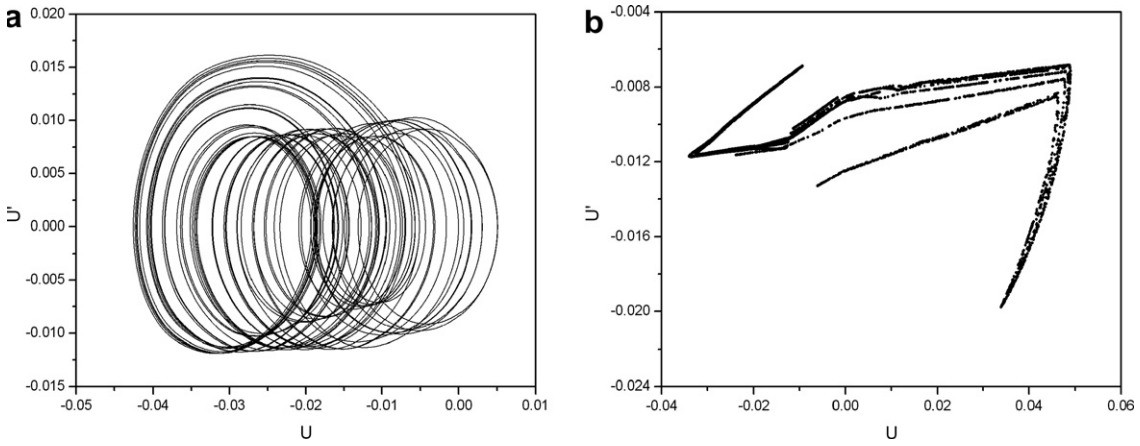

Fig. 19. Chaotic-like response: asymmetric case.

conditions are used, showing the attractor coexistence in Fig. 16(a) and (b). Notice that symmetric characteristic is broken and negative attractor becomes smaller than the positive one.

Transient responses and multi-stability are still present in this asymmetric system and the forthcoming analysis exploits this coexisting attractors multi-stability by changing initial conditions and assuming $\delta = 4 \times 10^{-3}$, $\varpi = 1$ and $\xi = 5 \times 10^{-6}$. By assuming initial conditions within the cloud of points presented in Fig. 16(a), a chaotic-like response occurs, being related to oscillations in the positive part of phase space (called positive chaotic-like response) (Fig. 17). On the other hand, by assuming initial conditions within the other cloud (Fig. 16(b)), the system presents a negative chaotic-like response that occurs in the negative part of phase space (Fig. 18).

By considering a chaotic-like response related to the bifurcation diagram region with the same characteristics for both initial conditions (regions of Fig. 16(a) and (b) for $\delta > 9 \times 10^{-3}$, for instance, $\delta = 9.5 \times 10^{-3}$), the attractor is associated with the whole state space (including positive and negative parts). Nevertheless, it should be pointed out that chaotic attractor has a different form (Fig. 19), when compared to the symmetric case shown in Fig. 11.

5. Conclusions

This contribution analyzes the dynamical response of a single-degree of freedom shape memory alloy mechanical oscillator where the restitution force is described through a constitutive model with internal constraints. This model captures the general thermomechanical behavior of SMAs, allowing the description of various aspects of the dynamical system, including tensile-compressive asymmetry. An iterative numerical procedure is developed based on the operator split technique. Under this assumption, coupled governing equations are solved from uncoupled problems, where classical numerical methods can be employed. The fourth-order Runge–Kutta method is employed together with the orthogonal projection algorithm, used to solve the constitutive equations. Results of numerical simulations indicate that this system has a rich behavior with different kinds of responses. An important characteristic of these systems is the equilibrium point temperature dependence, which means that the number and the characteristic of equilibrium points changes with the temperature. This behavior allows one to imagine changes of system position with temperature variation. Other interesting characteristic of SMA oscillator is the adaptive dissipation due to the hysteresis loop that can be exploited in passive vibration control. Finally, it should be pointed out the possibility of SMA system to perform many types of behaviors, which can be exploited in the sense of giving flexibility to the system. Among various kinds of response, SMA oscillator may present chaotic-like response and also attractors multi-stability. Therefore, the response of SMA devices subjected to dynamic loadings can be very complex being of special interest to be accurately investigated.

Acknowledgement

The authors acknowledge the support of the Brazilian Agency CNPq.

References

[1] Baêta-Neves AP, Savi MA, Pacheco PMCL. On the Fremond's constitutive model for shape memory alloys. Mech Res Commun 2004;31(6):677–88.
[2] Bernardini D, Rega G. Thermomechanical modelling, nonlinear dynamics and chaos in shape memory oscillators. Math Comput Modell Dyn Syst 2005;11(3):291–314.
[3] Birman V. Review of mechanics of shape memory alloy structures. Appl Mech Rev 1997;50:629–45.
[4] Cai W, Lu XL, Zhao LC. Damping behavior of TiNi-based shape memory alloys. Mater Sci Eng A 2005;394:78–82.
[5] Collet M, Foltête E, Lexcellent C. Analysis of the behavior of a shape memory alloy beam under dynamical loading. Eur J Mech A – Solids 2001;20:615–30.
[6] Denoyer KK, Scott Erwin R, Rory Ninneman R. Advanced smart structures flight experiments for precision spacecraft. Acta Astronaut 2000;47:389–97.
[7] Feng ZC, Li DZ. Dynamics of a mechanical system with a shape memory alloy bar. J Intell Mater Syst Struct 1996;7:399–410.
[8] Gandhi F, Chapuis G. Passive damping augmentation of a vibrating beam using pseudoelastic shape memory alloy. J Sound Vib 2002;250(3):519–39.
[9] Garner LJ, Wilson LN, Lagoudas DC, Rediniotis OK. Development of a shape memory alloy actuated biomimetic vehicle. Smart Mater Struct 2001;9(5):673–83.
[10] Han Y-L, Xing D-J, Xiao E-T, Li A-Q. NiTi-Wire shape memory alloy dampers to simultaneously damp tension, compression, and torsion. J Vib Control 2005;11(8):1067–84.
[11] Kibirkstis E, Liaudinskas R, Pauliukaitis D, Vaitasius K. Mechanisms with shape memory alloy. J Phys IV 1997;C5:633–6.
[12] Lacarbonara W, Vestroni F. Nonclassical responses of oscillators with hysteresis. Nonlinear Dyn 2003;32:235–58.
[13] Lacarbonara W, Bernardini D, Vestroni F. Nonlinear thermomechanical oscillations of shape-memory devices. Int J Solids Struct 2004;41(5–6):1209–34.
[14] Lagoudas DC, Khan MM, Mayes JJ, Henderson BK. Pseudoelastic SMA spring elements for passive vibration isolation: Part II – Simulations and experimental correlations. J Intell Mater Syst Struct 2004;15(6):443–70.
[15] Machado LG, Savi MA. Odontological applications of shape memory alloys. Rev Bras Odontologia 2002;59(5):302–6 [in Portuguese].
[16] Machado LG, Savi MA. Medical applications of shape memory alloys. Braz J Med Biol Res 2003;36(6):683–91.
[17] Machado LG, Savi MA, Pacheco PMCL. Nonlinear dynamics and chaos in coupled shape memory oscillators. Int J Solids Struct 2003;40(19):5139–56.
[18] Machado LG, Savi MA, Pacheco PMCL. Bifurcations and crises in a shape memory oscillator. Shock Vib 2004;11(2):67–80.
[19] Mosley MJ, Mavroidis C. Experimental nonlinear dynamics of a shape memory alloy wire bundle actuator. J Dyn Syst Meas Control 2001;123:103–23.
[20] Oberaigner ER, Fischer FD, Tanaka K. On the optimal damping of a vibrating shape memory alloy rod. J Eng Mater Technol – ASME 2002;124:97–102.
[21] Ortiz M, Pinsky PM, Taylor RL. Operator split methods for the numerical solution of the elastoplastic dynamic problem. Comput Meth Appl Mech Eng 1983;39:137–57.
[22] Pacheco PMCL, Savi MA. A non-explosive release device for aerospace applications using shape memory alloys. In: Proceedings of XIV the Brazilian congress of mechanical engineering (COBEM 97 – ABCM), Bauru, Brazil, 1997.
[23] Paiva A, Savi MA. An overview of constitutive models for shape memory alloys. Mathematical Problems in Engineering 2006;2006:1–30. Article ID56876.
[24] Paiva A, Savi MA, Braga AMB, Pacheco PMCL. A constitutive model for shape memory alloys considering tensile-compressive asymmetry and plasticity. Int J Solids Struct 2005;42(11–12):3439–57.
[25] Pietrzakowski M. Natural frequency modification of thermally activated composite plates. Mec Ind 2000;1:313–20.
[26] Rockafellar RT. Convex analysis. New Jersey: Princeton Press; 1970.
[27] Rogers CA. Intelligent materials. Scientific American 1995(September):122–7.
[28] Saadat S, Noori M, Davoodi H, Hou Z, Suzuki Y, Masuda A. Using NiTi SMA tendons for vibration control of coastal structures. Smart Mater Struct 2001;10:695–704.
[29] Saadat S, Salichs J, Noori M, Hou Z, Davoodi H, Bar-On I, et al. An overview of vibration and seismic applications of NiTi shape memory alloy. Smart Mater Struct 2002;11(2):218–29.
[30] Salichs J, Hou Z, Noori M. Vibration suppression of structures using passive shape memory alloy energy dissipation devices. J Intell Mater Syst Struct 2001;12(10):671–80.
[31] Savi MA, Paiva A. Describing internal subloops due to incomplete phase transformations in shape memory alloys. Arch Appl Mech 2005;74(9):637–47.
[32] Savi MA, Braga AMB. Chaotic vibrations of an oscillator with shape memory. J Braz Soc Mech Sci Eng 1993;XV(1):1–20.
[33] Savi MA, Braga AMB. Chaotic response of a shape memory oscillator with internal constraints. In: Proceedings of XII the Brazilian congress of mechanical engineering (COBEM 93 – ABCM), Brasília, Brazil, 1993. p. 33–6.
[34] Savi MA, Pacheco PMLC. Chaos and hyperchaos in shape memory systems. Int J Bifurcat Chaos 2002;12(3):645–57.
[35] Savi MA, Pacheco PMLC, Braga AMB. Chaos in a shape memory two-bar truss. Int J Non-linear Mech 2002;37(8):1387–95.
[36] Savi MA, Paiva A, Baêta-Neves AP, Pacheco PMCL. Phenomenological modeling and numerical simulation of shape memory alloys: a thermo-plastic-phase transformation coupled model. J Intell Mater Syst Struct 2002;13(5):261–73.

[37] Schmidt I, Lammering R. Experimental investigation on the damping behaviour of superelastic NiTi. J Phys IV 2004;115:11–20.
[38] Seelecke S. Modeling the dynamic behavior of shape memory alloys. Int J Non-linear Mech 2002;37(8):1363–74.
[39] Sun S, Rajapakse RKND. Simulation of pseudoelastic behaviour of SMA under cyclic loading. Comput Mater Sci 2003;28:663–74.
[40] van Humbeeck J. Non-medical applications of shape memory alloys. Mater Sci Eng A 1999;273–275:134–48.
[41] van Humbeeck J. Damping capacity of thermoelastic martensite in shape memory alloys. J Alloys Compd 2003;355:58–64.
[42] Williams K, Chiu G, Bernhard R. Adaptive-passive absorvers using shape-memory alloys. J Sound Vib 2002;249(5):835–48.
[43] Webb G, Wilson L, Lagoudas DC, Rediniotis O. Adaptive control of shape memory alloy actuators for underwater biomimetic applications. AIAA J 2000;38(2):325–34.